Journal of Colloid and Interface Science 665 (2024) 10–18

Contents lists available at ScienceDirect

Journal of Colloid And Interface Science

journal homepage: www.elsevier.com/locate/jcis

Regular Article

Biochar from olive tree twigs and spent malt rootlets as electrodes in Zn-air batteries

Theodoros Kottis [a], Nikolaos Soursos [a], Katerina Govatsi [b], Lamprini Sygellou [c], John Vakros [a,*], Ioannis D. Manariotis [d], Dionissios Mantzavinos [a], Panagiotis Lianos [a,*]

[a] Department of Chemical Engineering, University of Patras, 26500 Patras, Greece
[b] Laboratory of Electron Microscopy and Microanalysis, School of Natural Sciences, University of Patras 26500 Greece
[c] Foundation of Research and Technology – Institute of Chemical Engineering Science (FORTH/ICE-HT), Stadiou Str. Platani, P.O. Box 1414, Patras 26500, Greece
[d] Department of Civil Engineering, Environmental Engineering Laboratory, University of Patras, University Campus 26500 Patras, Greece

GRAPHICAL ABSTRACT

for the manuscript for the manuscript JCIS-24–2223 "Biochar from olive tree twigs and spent malt rootlets as electrodes in Zn-air batteries", by Kottis et al.

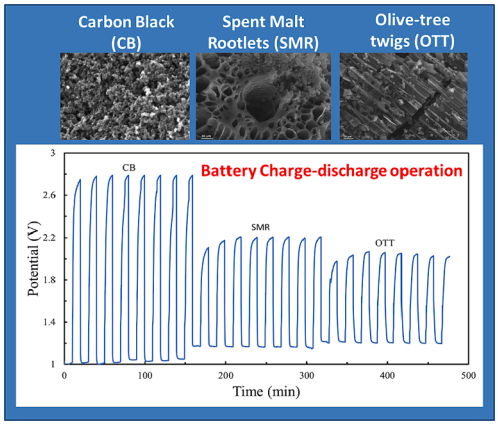

ARTICLE INFO

Keywords:
Biochar
Biochar activation
Olive-Tree Twigs
Spent Malt Rootlets
Zn-air batteries
Electrocatalysis

ABSTRACT

Biochars, i.e. porous carbons obtained by pyrolysis of biomass, can act as electrocatalysts for oxygen evolution and oxygen reduction reaction. In the present work, two biochars have been prepared by using materials of completely different biomass origin: olive-tree twigs and spent malt rootlets (brewery wastes). Both biomass species were subjected to pyrolysis under limited oxygen supply and then they were activated by mixing with KOH and pyrolysis again. The obtained biochars were characterized by several techniques in order to determine their structural characteristics and the composition of their active components. Despite their different origin, the two biochars demonstrated similar structural and compositional characteristics thus highlighting the importance of the pyrolysis and activation procedure. Both biochars were used as electrocatalysts in the operation of rechargeable Zn-air batteries, where they also demonstrated similar electrocatalytic capacities with only a small

* Corresponding authors.
E-mail addresses: vakros@chemistry.upatras.gr (J. Vakros), lianos@upatras.gr (P. Lianos).

https://doi.org/10.1016/j.jcis.2024.03.114
Received 13 February 2024; Received in revised form 14 March 2024; Accepted 17 March 2024
Available online 18 March 2024

advantage gained by olive-tree-twigs biochar. Compared to bare nanoparticulate carbon (carbon black), both biochars demonstrated a marked advantage towards oxygen evolution reaction.

1. Introduction

Zn-air batteries are recently studied with great interest as alternative means of energy storage [1–10]. One of the main functions in the operation of Zn-air and, generally, metal-air batteries is the oxygen reduction reaction (ORR) at the air (cathode) electrode. The metal anode is easily oxidized, particularly in a highly alkaline environment, liberating electrons. For the battery to properly function, these electrons must be carried through an external circuit and consumed at the air electrode by oxygen reduction. The consumption of electrons must be very efficient, otherwise, they are stacked, and instead of oxygen, they reduce water producing hydrogen. This is an undesirable side-effect. Oxygen can be reduced by one of the following $2e^-$ or $4e^-$ reactions (written for an alkaline environment):

$$O_2 + 2e^- + 2H_2O \rightarrow H_2O_2 + 2OH^- \quad (1)$$

$$O_2 + 4e^- + 2H_2O \rightarrow 4OH^- \quad (2)$$

It is obvious that reaction (2) is preferred in order to consume more electrons; however, this $4e^-$ reaction is only possible in the presence of an efficient electrocatalyst. Nanoparticulate Pt is the obvious choice for an efficient electrocatalyst, but this metal is very expensive and also suffers from agglomeration and sulfur poisoning that may deactivate it [11,12]. Therefore, it is necessary to search for alternative electrocatalysts. ORR is not only important for metal-air batteries but also for any other device that depends on an air–cathode, including hydrogen fuel cells, microbial fuel cells, etc. For this reason, the research community has undertaken a huge effort to develop alternative ORR electrocatalysts. In the case of rechargeable Zn-air batteries, the electrocatalyst on the air electrode should additionally facilitate the oxygen evolution reaction (OER). Indeed, when a Zn-air battery is charged, the flow of electrons is reversed, i.e., it takes place from the air electrode to the metal electrode. This results in water oxidation and oxygen evolution at the air electrode, i.e., the reversal of reaction (2). In order for the reversal of reaction (2) to be efficient, it is again necessary to employ an efficient electrocatalyst. Electrocatalysts then employed with rechargeable Zn-air batteries should be bifunctional and should facilitate both ORR and OER. This calls for further studies and is responsible for further intensification of the related research [3–5,13–22].

The three basic properties of an efficient electrocatalyst are the following: (1) it should be made of an electrically conductive material so as to allow the transfer of charges from the solid to the fluid phase; (2) it should possess a high active area in order to increase the interface between the solid and the fluid phase; and (3) it should possess active sites that would again facilitate the transfer of charges between the two phases. Any serious electrocatalyst should demonstrate such properties. Fortunately, in recent years, it has been realized that all three basic properties may be simultaneously possessed by a material that is abundantly available and can be easily processed. This is biochar, i.e. carbon, which can be obtained by pyrolysis of wastes of biological origin, both from plants and animals, with the advantage of almost unlimited selection of the raw biomass to obtain biochars of different origins [17,23–27].

The standard route to make activated biochar is to dry biomass, mix it with KOH, dry again, and pyrolyze the mixture in an oxygen deficient atmosphere. Variants of this process have also appeared in the literature [17,23,24,27–31]. This treatment may lead to the evaporation of all volatile components, leaving behind only carbon. The presence of KOH leads to the decomposition of lignin, thus ensuring that the final material is active carbon and does not contain inactive residues. The final material is highly porous, with a hierarchical distribution of micro, *meso*, and macro pores. Porosity is necessary in order to increase the specific surface. The hierarchy in pore distribution is also necessary in order to facilitate ion dispersion through the pores. Activated biochar is recorded to reach very high specific surfaces, in some cases over 1000 m^2/g [29,32,33]. Because of its electric conductivity and its high specific surface, activated biochar has been repeatedly studied as a material for making supercapacitors [29,32–39], that operate by the formation of a Helmholtz double layer in the presence of an electrolyte. Nevertheless, biochars are naturally enriched with active sites, such as O, N, S, P, etc., depending on the origin of the biomass. Furthermore, it is always possible to enrich biochar with active sites through additional treatment. In any case, such biochars possess the three above basic properties of an electrocatalyst, i.e., they are electrically conductive, because of carbon, they have a high specific surface, because of their porosity, which is additionally hierarchical, and they contain active sites. Indeed, biochars have been recently studied as electrocatalysts, and they have subsequently been applied to the construction of Zn-air batteries [4,5,15–17,19]. It must be also added at this point that in recent years there has been an explosive interest in the use of biochar for environmental remediation purposes, thanks to its ability to adsorb environmentally harmful agents, and this has promoted biochar as one of the most interesting materials of our days [31,39–41]. Furthermore, its catalytic capacity is not limited to electrocatalysis but it is also valuable as catalyst in a wide range of processes, including among others oxidation of organic components and transesterification [42,43]. Even though, other carbon materials may be used as catalysts [44–46], biochar is more attractive, since it is the product of valorization of spent biomass.

The electrocatalytic functionality of biochars has also been examined in the present work. More specifically, we have studied two biochars derived from two common materials originating from biomass, which would otherwise be disposed of as waste: olive-tree twigs (i.e. small branches from olive trees, OTT) and spent malt rootlets (SMR). Olive-tree twigs are either burned or disposed of, while SMR are brewery waste. Our specific purpose was to investigate the presence of heteroatoms in biochars of various origins, assess their variation from one species to the other, and finally study their electrocatalytic ORR and OER capacities.

2. Experimental

2.1. Materials

All reagents were supplied by Sigma-Aldrich, unless otherwise specified. Thus, carbon cloth (CC) was from Fuel Cell Earth (Wobum, MA, USA) and carbon black (CB) from Cabot Corporation (Vulcan XC72, Billerica, MA, USA).

2.2. Preparation of the biochar and the electrodes

The biochar was prepared from either spent malt rootlets, the main byproduct of the Athenian Brewery S.A (Patras, Greece) or from olive-tree twigs, collected from local olive trees. Both of these materials have high lignin content, and they are expected to yield a highly specific surface after lignin removal [47].

A weighed quantity of the dried rootlets or ground dry olive-tree twigs was placed in a quartz vessel and pyrolyzed at 850 °C in a gradient temperature furnace (LH 60/12, Nabertherm GmbH, Germany) under limited air supply, containing 20 % of the oxygen that would have been necessary to completely burn the biomass. The heating and cooling

rate was 10 °C per min. The obtained powders were further treated by mixing them with KOH. The mixture contained 3 parts of KOH and 1 part of biochar (by weight). Then it was again placed in a quartz vessel and heated again at 850 °C, as above. Finally, the obtained material was washed and filtered a few times, and at the end, it was dried for 2 h at 80 °C in a vacuum furnace (Nüve, EV018). This final product was used to make electrodes. Electrodes were made of carbon cloth with biochar deposited on it. To do so, 0.27 g of biochar, 0.03 g of carbon black, and 5 mL of isopropanol were vigorously mixed in a homogenizer (Silverson L5M) until a uniform dispersion was formed. Then 0.1 g of polytetrafluoroethylene (60 % wt. dispersion in water) was added to this dispersion, sonicated for 30 min, and homogenized again until a uniform suspension was again obtained. A layer of this suspension was then deposited onto a carbon cloth of active dimension 1 cm × 1 cm by doctor blading. The cloth was then dried at 80 °C for 30 min and calcined at 340 °C for 1 h. This procedure was repeated for a second time to ensure uniform deposition of the biochar on the carbon cloth and load approximately the same amount of material, which was 30 mg (OTT/CC or SMR/CC electrodes). In addition, an electrode made only with carbon black on carbon cloth (CB/CC) has also been constructed by mixing 0.3 g of CB with 5 mL of isopropanol and by following the rest of the above procedure. Care was taken to deposit the same quantity of CB on CC, i.e. 30 mg, as in the case of biochar electrodes.

2.3. Characterizations

Electron microscopy images for characterizing the morphologies of the prepared powders were recorded with a Scanning Electron Microscope (SEM) (JEOL, JSM-6300) operating at 20 kV, equipped with an X-ray Energy Dispersive Spectrometer (EDX) (Oxford). Surface analysis measurements were performed in a UHV chamber ($P \sim 5 \times 10^{-10}$ mbar) equipped with a SPECS Phoibos 100-1D-DLD hemispherical electron analyzer and a non-monochromatized dual-anode Mg/Al x-ray source. The XP Spectra were recorded with MgKα ($h\nu = 1253.6$ eV) and an analyzer pass energy of 15 eV giving a Full Width at Half Maximum (FWHM) of 0.85 eV for the Ag3d5/2 line. The analyzed area was a spot of 3 mm diameter. For spectra collection and treatment, including fitting, the commercial software SpecsLab Prodigy (Specs GmbH, Berlin) was used. The XP core level peaks were deconvoluted with a mixed Gaussian – Lorentzian functions after a Shirley background subtraction. The samples were in powder form and were pressed on an In foil.

The specific surface area (SSA) of the samples was determined by using the BET equation from N_2 adsorption isotherms at liquid N_2 temperature and by using a Tristar 3000 porosimeter, Micromeritics. The micropore surface area was determined by using the *t*-plot method. X-ray diffraction (XRD) patterns were recorded using a Bruker D8 Advance diffractometer equipped with a nickel-filtered CuKa (1.5418 Å) radiation source and the Fourier transform infrared (FTIR) spectrum was recorded at 4000–400 cm^{-1} using a Perkin Elmer Spectrum RX FTIR system with a KBr pellet and with 1 % w/w biochar.

All electrochemical measurements were carried out with an Autolab potentiostat PGSTAT128N (Utrecht, The Netherlands).

2.4. Electrochemical characterization of the electrodes

Water oxidation and oxygen reduction capacity of the biochar and CB electrodes were studied in a three-electrode cell by employing biochar or CB electrode as the working electrode, a Pt wire as the counter electrode and Ag/AgCl as the reference electrode. The electrolyte was aqueous 0.5 M NaOH. Water oxidation was studied in linear sweep voltametry by scanning voltage from 0 to 1.2 V vs Ag/AgCl. Oxygen reduction was studied in an oxygen saturated solution by scanning voltage from 0 to −1.0 V vs Ag/AgCl. The obtained data were plotted against Reversible Hydrogen Electrode (RHE) by taking into account the potential of the Ag/AgCl electrode (approximately 0.2 V) and the pH of the 0.5 M NaOH solution (~13).

2.5. Construction and operation of the Zn-air battery

Zn-air batteries were constructed by using a Zn foil (Alfa Aesar) anode and an OTT/CC, SMR/CC or CB/CC cathode electrode. The distance between the two electrodes was 5 mm and the electrolyte was 5 M NaOH containing 0.2 M ZnO [9]. All measurements were carried out by employing the above mentioned Autolab potentiostat.

3. Results and discussion

3.1. Structural characterization of the OTT and SMR biochars

The two samples studied in this work were first characterized by SEM and EDX analysis. SEM images are shown in Fig. 1 revealing a characteristic tubular structure in the case of OTT. The tubes were all about the same diameter. After KOH treatment, the tubes were broken but approximately kept the same diameter. In the case of SMR, tubular pores were again observed, but they were dispersed in a hierarchical distribution of sizes, i.e. pores attained dimensions of various sizes, from very small to very large.

Subsequent EDX analysis showed the atomic percentage composition of the two biochars (after KOH treatment). The results are shown in Table 1. The table reveals the predominant presence of C and O. Potassium is expected as a residue of the KOH treatment. In addition, only traces of Ca were detected in OTT and traces of P in SMR. This information was further enriched by XPS analysis.

From the XPS Survey scans of OTT and SMR samples (not shown), Carbon, Oxygen, Silicon, Calsium and Magnesium have been detected. Additionally, potassium was detected on SMR, while phosphorus and nitrogen were again found only on the SMR sample. From the peak area of the detailed C1s, O1s, K2p, Si2p, Ca2p, P2p, Mg2p and N1s peaks divided by relative sensitivity factors (based on Scofield RSF and the energy analyzer transmission function), the % atomic concentration can be derived and is presented in Table 2. Furthermore, Fig. 2 shows the C1s-K2p XPS combined window, where the C1s peak is analyzed into six components attributed to C—C sp^2 and sp^3 hybridization, hydroxyls, carbonyls, carboxyls and carbonates, in accordance with previously reported data [48]. The % component concentration and the binding energies of each component are shown in Table 3. The C—C sp^2 (C═C) bonding, responsible for electric conductivity in carbon, attained a predominant percentage in both biochars (55.7 % in OTT and 59.4 % in SMR).

The adsorption and desorption isotherms at liquid nitrogen temperature for the two activated biochars can be seen in Fig. 3. Both OTT and SMR attained high values of specific surface area, i.e. 1020 and 1140 m^2g^{-1}, respectively, the micropores surface area were 610 and 690 m^2g^{-1}, while the corresponding pore volumes were 0.62 and 0.99 mLg^{-1}, respectively. This was an expected result since the KOH activation procedure has been repeatedly proven to be a powerful tool for increasing the SSA of biochar [31]. Indeed the SSA for the two biochars before KOH treatment was only 89 and 100 m^2g^{-1}, for OTT and SMR, respectively. As it was reported in a previous work [49], the various components found in raw biomass, like cellulose, hemicellulose and lignin, considerably influence the properties of the carbon phase after pyrolysis, especially at 850 °C. This high temperature can cause severe transformation of the carbonaceous phase during pyrolysis, although it is not completed. Thus various parts of the carbonaceous phase may react with base or acid solutions. Especially the carbon phase of lignin is sensitive to bases while the carbon phase from cellulose and hemicellulose can react with acid solutions. The main component of the two presently used raw biomass samples is lignin, thus part of the lignin and the lignin-based carbon phase can react with bases, be dissolved, and thus be removed. [49]. During the pyrolysis procedure, KOH melts, facilitating the reaction with lignin-derived components. Consequently, both activated OTT and SMR attained high SSA and pore volume as expected. Fig. 3 shows that the two biochars have an hierarchical

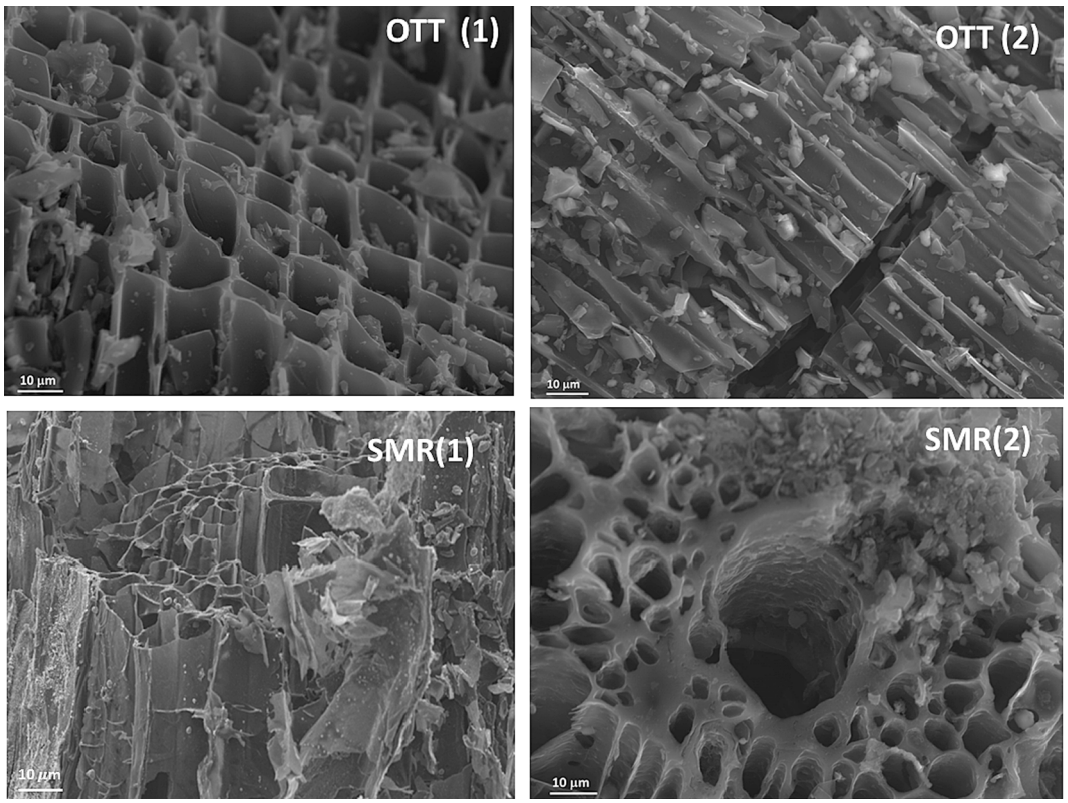

Fig. 1. SEM images of the OTT and SMR biochar powders before (1) and after (2) KOH treatment.

Table 1
Atomic percent of elements detected by EDX analysis on samples treated with KOH.

Sample	C	O	K	P	Ca
OTT	85.3	13.2	0.4	–	1.1
SMR	84.6	9.2	5.9	0.3	–

Table 2
% surface atomic concentration of OTT and SMR biochar samples as derived from the XPS analysis. Data recorded with 0.5% error.

XPS Peak	Eb [eV]	Assignements	OTT	SMR
C1s	284.5	C–C	85.4	63.6
Ca2p	347.7	$CaCO_3$	0.5	1.9
O1s	532.5	Mainly C–O	9.6	20.7
K2p	293.0	K_2CO_3	–	3.0
Si2p	103.2	SiO_2	1.0	2.3
P2p	~135	H_3PO_4	–	1.6
Mg2p	51.5	$Mg(OH)_2$	3.5	4.8
N1s	401.2	N–C	–	2.1

structure. Pores can be determined in all three dimensions, micropores (with diameter lower than 2 nm), mesopores (with diameter between 2 and 50 nm) and macropores with diameter higher than 50 nm. Interestingly, there are a few differences between the two biochars. Although the majority of the pores are located in the microporous region, the OTT biochar had a limited amount of macropores in contrast to the SMR. The mesopores were rather smaller in the case of OTT. They had a mean diameter of 18 nm while in the case of SMR the mean diameter was higher and estimated about 38 nm.

The XRD patterns of the two biochars are presented in Fig. 4. The SMR biochar had a low-intensity XRD pattern in contrast with the OTT biochar. As seen in Fig. 4, where the SMR XRD pattern is magnified, both biochars possess the two main broad peaks centered at about 23.5° and 42°, corresponding to C(0 0 2) and C(1 0 0). The first can be assigned to the (0 0 2) crystal plane of hard carbon in lignocellulose form [50]. This peak is typical of a carbonaceous material with a less ordered structure due to pyrolysis (amorphous graphitic phase). In our case, this peak is broad in the SMR biochar. This can be evidence that KOH can interact in a higher degree with the SMR biochar and dissociate the graphitic layers better in contrast with the OTT biochar. The second peak is due to sp^2 carbons and is closely related to the electrical conductivity of the biochar [51]. Both biochars then contain a substantial percentage of sp^2 carbons, in accordance with the data in Table 3. The only peak that corresponds to an inorganic phase is the one at about 31°, describing potassium carbonate species.

Finally, the FTIR spectra of the two biochars are presented in Fig. 5. The main band in both biochars is the intense band centered at about 1380 cm^{-1}, due to carbonates. The exact position of this band can be influenced by many parameters, like the hydration ratio or the cation used for the formation of carbonates. In our case, the main compensating ion is K^+ [52], as was suggested from the EDX and XPS analysis. Other bands are due to C—O and –OH bonds centred at 1035 cm^{-1} and 3432 cm^{-1}, respectively, typical of the carbonaceous phase [53,54]. These bands are more intense in the case of SMR biochar. This is expected since the O content was higher in SMR.

The above physicochemical characterization techniques have shown that the activation procedure was successfully performed since the SSA of the biochars was increased more than ten times. Indeed, non-activated biochars have a moderate SSA of about 100 m^2g^{-1} or less. Although the activation pyrolysis was performed under intense conditions, these conditions tend to smooth out possible differences. The starting biomass had an impact on the physicochemical characteristics of the final biochar. Indeed, the SMR biochar has a higher content of O and K in contrast with the OTT. This means that the surface is more oxidized in SMR biochar. As a result, the SMR may exhibit more oxygen groups than the OTT. Although this is an interesting property for the

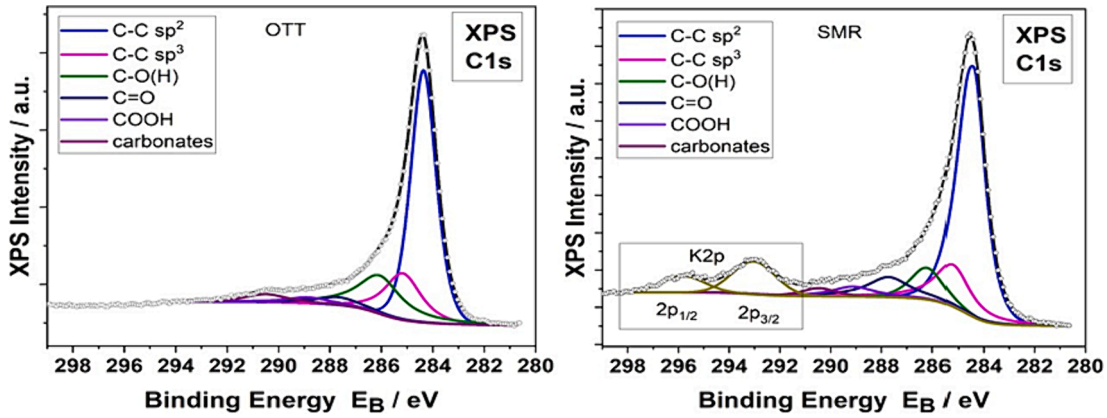

Fig. 2. Deconvoluted C1s XPS peak for the OTT and SMR biochars. K2p peak was detected only in SMR.

Table 3
% carbon component concentration derived from C1s XPS peak deconvolution of OTT and SMR biochar samples. Data recorded with 0.5 % error.

Eb (eV)	Assignments	OTT	SMR
284.4 ± 0.1	C–C sp^2	55.7	59.4
285.3 ± 0.1	C– C sp^3	15.5	15.2
286.2 ± 0.2	C–O(H)	18.6	8.5
287.8 ± 0.2	C═O	4.2	9.8
289.0 ± 0.2	COOH	3.2	4.8
290.5	carbonates	2.8	2.3

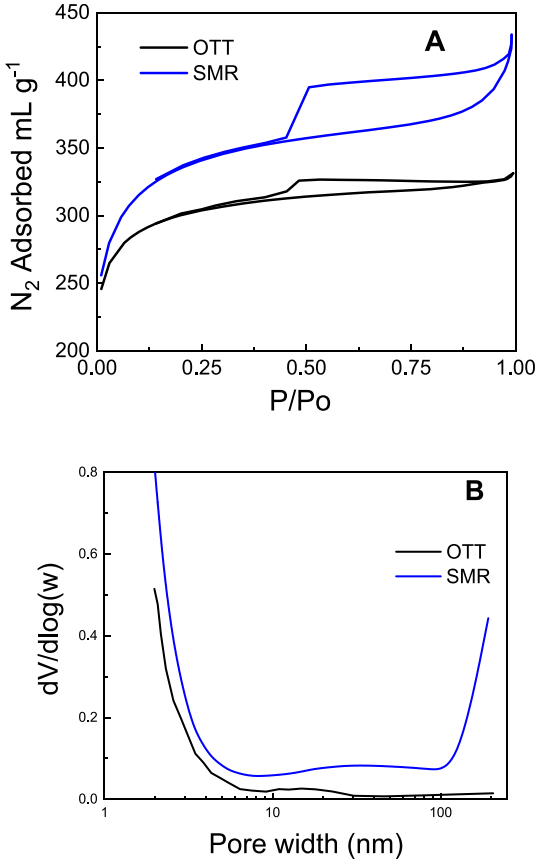

Fig. 3. N_2 adsorption–desorption isotherms at liquid nitrogen temperature (A) and pore widths (B) for the two biochars.

development of the double layer and the interaction with possible ions in the interface region, it is not expected to alter the electrical conductivity and thus the electrochemical properties of the biochar. Also, K content was higher in SMR, pointing out either that the surface can interact better with cations or that the activation procedure was more effective in SMR, probably due to the different raw biomass. This confirms that the reactivity of various carbon sources has a significant influence on the surface chemistry, which may further affect the performance of biochar as an electrode [55]. On the other hand, the higher amount of C in the OTT, as found by XPS analysis (85.4 % for OTT and 63.6 % for SMR), is expected to be beneficial for the conductivity. The XRD patterns is a first, although weak, evidence for this fact, since the peaks which correspond to C are more intense in the case of OTT. Interestingly, the ratio of the different non-oxidized forms of the surface carbon, namely C—C sp^3 and C═C sp^2, was not significantly different in the two biochars, although the percentage in OTT was higher. At this point, it should be noted that the activation procedure leads to biochars with a high point of zero charge, higher than 11, thus diminishing all possible effects due to surface charge. This is not crucial to our application since the charge is defined by the applied potential.

Various studies have been reported on the performance of biochar electrodes in many different applications including direct carbon fuel cell and supercapacitors [56–60]. The high specific surface area is a prerequisite for active electrocatalysts but the efficiency is not governed only by the surface area and the surface groups. To increase the efficiency, doping with heteroatoms has been applied. The heteroatoms are usually N, S and transition metal ions [61–63]. Although significant work has been performed in this field, comparison of different raw biomass under the same conditions are scarce.

In conclusion, SMR and OTT have some interesting differences, which originate from the different raw biomass. However, these differences are relatively small, since the intense pyrolysis conditions smooths them, and may or may not affect their application as electrocatalysts. An answer to this question is provided in the following subsection.

3.2. Electrocatalytic properties of the two biochars in comparison with carbon black

Electrodes made by depositing equal quantities of the two biochars on carbon cloth, as described in detail in the experimental section, were studied for their OER and ORR capacities in comparison with an electrode loaded with only carbon black. Fig. 6A and B show the results. In the case of oxidative electrocatalysis (Fig. 6A), both biochars demonstrated a marked difference from CB but a small difference between each other. Thus, the water oxidation threshold was approximately located at about 1.25 V vs RHE in the case of the two biochars, and the corresponding current increased fast after threshold in both OTT and SMR while in the case of CB substantial current was obtained only above 2.0 V

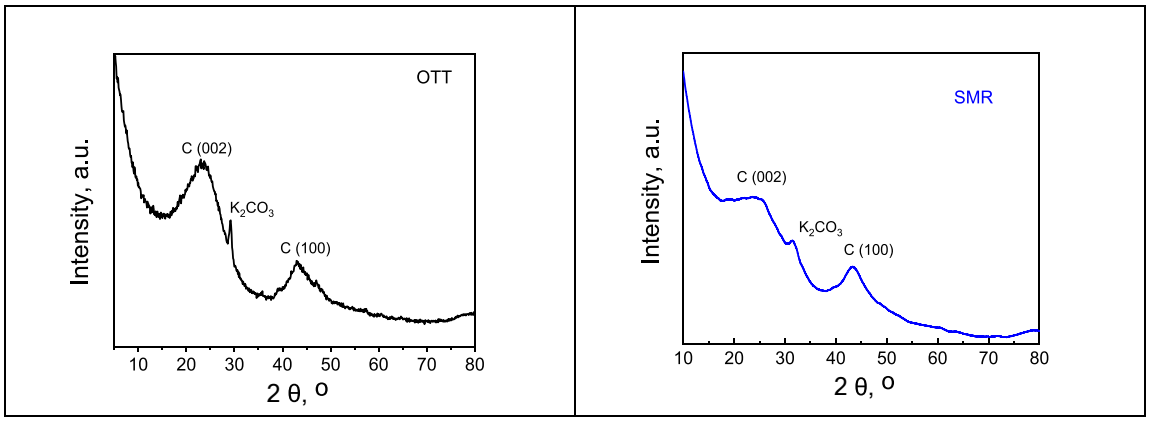

Fig. 4. XRD patterns of the two biochars.

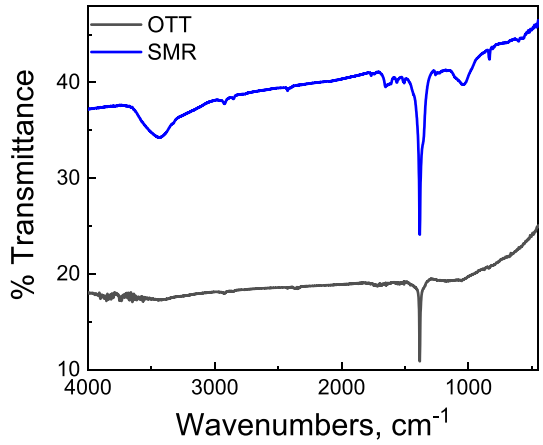

Fig. 5. FTIR spectra of the present biochars.

vs RHE. Obviously, the present biochars were much better OER electrocatalysts than nanoparticulate graphite (i.e. CB) but did not differentiate much between themselves. The small differences observed between the two biochars give an advantage to OTT, where the current increase is faster. In the case of reductive electrocatalysis (Fig. 6B), the differences between the three electrodes were smaller, with an advantage for the OTT biochar. It is concluded that the differences in the electrocatalytic capacity between the two biochars were relatively small with a slight advantage in the case of OTT biochar. Both biochars were much better OER electrocatalysts than carbon black, but in the case of ORR the differences between the three materials were smaller. In order to verify these conclusions, the above three electrodes have been employed as cathode electrodes in Zn-air batteries, as detailed in the following subsection.

3.3. Operation of the Zn-air battery

The functionality of a Zn-air battery was studied by employing Zn foil as anode and biochar or CB electrode as cathode. In order to distinguish the differentiation of behavior between the cells made by using the three different cathode electrodes, the devices were subjected to potentiometric measurements under galvanostatic conditions by consecutive charge–discharge cycles. This is demonstrated by the results presented in Fig. 7. In the case of the CB/CC cathode, the variation of the potential took place between 1.0 and 2.7 V for a constant current density of 10 mA cm^{-2}. The lower potential corresponds to the discharge voltage, while the higher potential corresponds to the voltage necessary to charge the battery with a constant current density of 10 mA cm^{-2}. In the case of the SMR/CC cathode electrode, the corresponding potentials were 1.2 and 2.2 V while in the case of the OTT/CC they were 1.3 and 2.0 V. It is obvious that both biochars produced higher potentials during discharging and necessitated lower voltages to charge the battery compared with the CB/CC cathode. In the same sense, a clear advantage has also been observed with the biochar obtained from olive-tree twigs. Even though the differences between the three electrodes are not impressive, they remain very important, and they may have very important technological consequences in the sense that the present biochars were only KOH-activated carbons and were not additionally treated. It must be underlined at this point that the above results are comparable with those reported by other researchers using cathode electrodes bearing a variety of metal-free, carbon-based electrocatalysts [15,17,64].

Fig. 7 is in accordance with the results of Fig. 6. Indeed, the differences between the three materials were relatively small, as far as the discharge voltage is concerned (i.e. the lower voltage in Fig. 7) and this is in accordance with the small differences observed in their ORR capacity, seen in Fig. 6B. It is reminded that discharge of the battery takes place by oxygen reduction at the carbon electrode. On the contrary, the difference in charging voltage between CB and the biochars (upper potential) was much larger, and this is in accordance with the data in Fig. 6A. The small advantage detected by OTT biochar, is also in accordance with the data in Fig. 6.

Despite the small difference between SMR and OTT, both the above characterization procedures and the present electrocatalytic data rather tend to highlight two materials of similar behavior as opposed to the fact that their biomass origin is entirely different. *In other words, the present data stress the importance of the preparation procedure rather than the biomass origin of the biochar.*

4. Conclusions

The two biochars of different biomass origin studied in the present work as electrocatalysts demonstrated similar behavior both in their electrocatalytic properties and their structural characteristics. Both biochars were obtained by pyrolysis followed by KOH activation. Activated biochars did not contain any important sites due to heteroatoms except for C═O and C—O species. Double-bonded carbon appeared at an equivalent percentage in the two samples (55.7 and 59.4 % for OTT and SMR, respectively), thereby ascribing similar electric conductivities. Specific surface areas were high in both cases (1020 and 1140 m^2g^{-1} for OTT and SMR, respectively), with a difference which is considered small. The ratio of sp^2 to sp^3 species was similar in the two samples, and in general, all recorded data did not manage to greatly differentiate the two materials despite their different origin. All these results highlight the importance of the treatment procedure vs. biomass origin itself; at least as far as electrocatalytic properties are concerned.

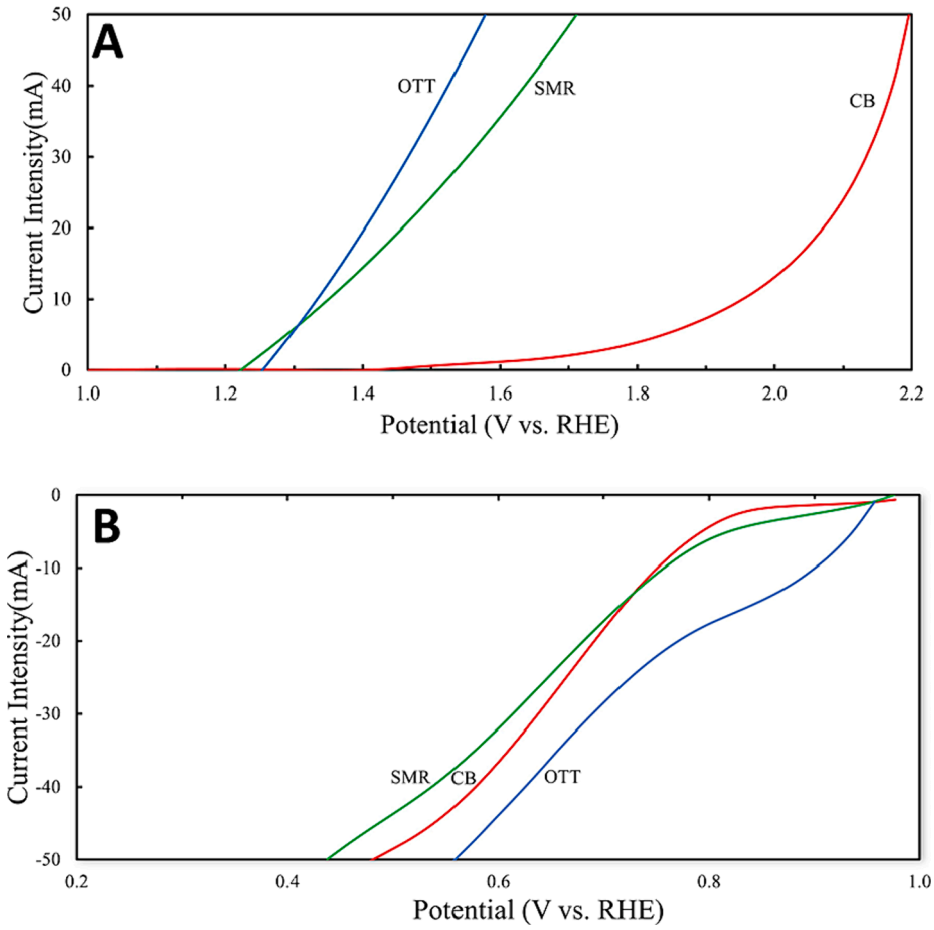

Fig. 6. Oxidative (A) and reductive (B) linear sweep voltametry using biochar or CB electrodes as the working electrode, a Pt wire as the counter electrode and Ag/AgCl as the reference electrode in a 0.5 M aqueous NaOH electrolyte.

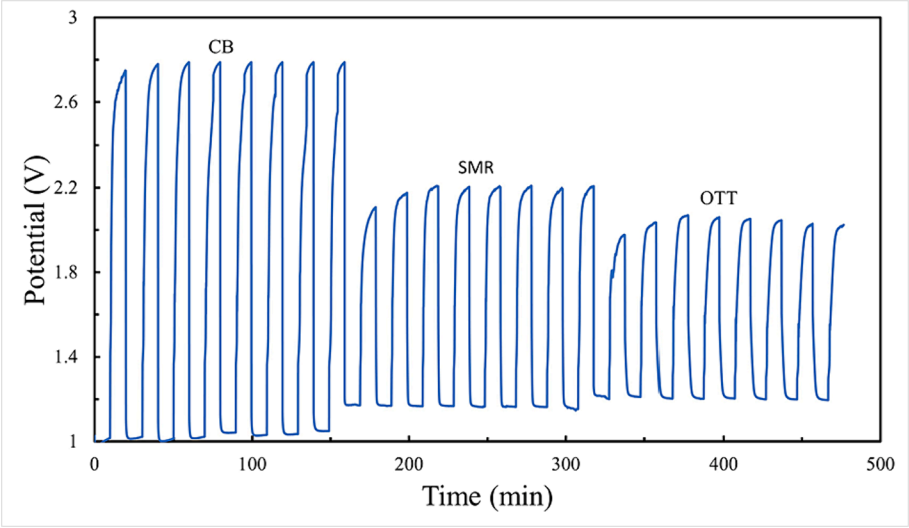

Fig. 7. Galvanostatic charge–discharge potentiometry with a Zn-air battery using cathode electrodes made of carbon cloth bearing CB, SMR or OTT electrocatalysts. The three cases were studied separately but they are plotted together for comparison. The current density was 10 mA cm^{-2}.

CRediT authorship contribution statement

Theodoros Kottis: Investigation. **Nikolaos Soursos:** Investigation. **Katerina Govatsi:** Investigation. **Lamprini Sygellou:** Writing – original draft, Investigation. **John Vakros:** Writing – original draft, Investigation, Conceptualization. **Ioannis D. Manariotis:** Writing – review & editing, Investigation. **Dionissios Mantzavinos:** Supervision. **Panagiotis Lianos:** Writing – review & editing, Supervision, Conceptualization.

Declaration of competing interest

The authors declare that they have no known competing financial interests or personal relationships that could have appeared to influence the work reported in this paper.

Data availability

No data was used for the research described in the article.

References

[1] Y. Li, H. Dai, Recent advances in zinc–air batteries chem, Soc. Rev. 43 (2014) 5257, https://doi.org/10.1039/C4CS00015C.

[2] P. Gu, M. Zheng, Q. Zhao, X. Xiao, H. Xue, H. Pang, Rechargeable zinc–air batteries: a promising way to green energy, J. Mater. Chem. A 5 (2017) 7651–7666, https://doi.org/10.1039/C7TA01693J.

[3] P. Lianos, A brief review on solar charging of Zn–air batteries, PCCP 25 (2023) 11883–11891, https://doi.org/10.1039/D3CP00307H.

[4] W. Shao, R. Yan, M. Zhou, L. Ma, C. Roth, T. Ma, S. Cao, C. Cheng, B. Yin, S. Li, Carbon-based electrodes for advanced zinc-air batteries: oxygen-catalytic site regulation and nanostructure design, Electrochemical Energy Reviews 6 (2023) 11, https://doi.org/10.1007/s41918-023-00181-x.

[5] C. Wang, S. Ran, W. Sun, Z. Zhu, Biomass-derived carbon materials with controllable preparation and their applications in zinc-air batteries: a mini review, Electrochem. Commun. 154 (2023) 107557, https://doi.org/10.1016/j.elecom.2023.107557.

[6] R. Sharma, H. Kumar, G. Kumar, S. Sharma, R. Aneja, A.K. Sharma, R. Kumar, P. Kumar, Progress and challenges in electrochemical energy storage devices: fabrication, electrode material, and economic aspects, Chem. Eng. J. 468 (2023) 143706, https://doi.org/10.1016/j.cej.2023.143706.

[7] J. Yi, Y. Xia, Advanced aqueous batteries: status and challenges, MRS Energy & Sustainability 9 (2022) 106–128, https://doi.org/10.1557/s43581-022-00033-z.

[8] O. Ola, N. Wang, G. Walker, Y. Zhu, D. Grant, Engineering the next generation of photorechargeable zinc-air batteries, Curr. Opin. Electrochem. 35 (2022) 101040, https://doi.org/10.1016/j.coelec.2022.101040.

[9] M. Katsaiti, E. Papadogiannis, V. Dracopoulos, A. Keramidas, P. Lianos, Solar charging of a zn-air battery, J. Power Sources 555 (2023) 232384, https://doi.org/10.1016/j.jpowsour.2022.232384.

[10] A. Iqbal, O.M. El-Kadri, N.M. Hamdan, Insights into rechargeable zn-air batteries for future advancements in energy storing technology, J. Storage Mater. 62 (2023) 106926, https://doi.org/10.1016/j.est.2023.106926.

[11] F. Maillard, S. Schreier, M. Hanzlik, E.R. Savinova, S. Weinkaufb, U. Stimming, Influence of particle agglomeration on the catalytic activity of carbon-supported pt nanoparticles in CO monolayer oxidation, PCCP 7 (2005) 385–393, https://doi.org/10.1039/B411377B.

[12] H. Ohtsuka, The oxidation of methane at low temperatures over zirconia-supported pd, ir and pt catalysts and deactivation by sulfur Poisoning, Catal. Lett. 141 (2011) 413–419, https://doi.org/10.1007/s10562-010-0506-x.

[13] W. Fanga, J. Zhaoa, W. Zhanga, P. Chen, Z. Baia, M. Wu, Recent progress and future perspectives of flexible zn-air batteries, J. Alloy. Compd. 869 (2021) 158918, https://doi.org/10.1016/j.jallcom.2021.158918.

[14] X. Wang, G.L. Li, Z.F. Lu, S. Cao, C. Hao, S. Wang, G. Sun, In situ coating of a N, S co-doped porous carbon thin film on carbon nanotubes as an advanced metal-free bifunctional oxygen electrocatalyst for Zn–air batteries, Cat. Sci. Technol. 120 (2022) 181, https://doi.org/10.1039/D1CY01818C.

[15] X. Xiao, X. Lia, Z. Wang, G. Yan, H. Guo, Q. Hu, L. Li, Y. Liu, J. Wang, Robust template-activator cooperated pyrolysis enabling hierarchically porous honeycombed defective carbon as highly-efficient metal-free bifunctional electrocatalyst for zn-air batteries, Appl Catal B 265 (2020) 118603, https://doi.org/10.1016/j.apcatb.2020.118603.

[16] M. Tan, Q. Wang, S. Wang, W. Liu, D. Wang, S. Luo, P. Hou, M. Zhou, Y. Zhang, S. Yan, X. Liu, Ternary (N, B, F)-doped Biocarbon derived from bean residues as efficient bifunctional electrocatalysts for oxygen reduction and evolution reactions, J. Electrochem. Soc. 169 (2022) 096517, https://doi.org/10.1149/1945-7111/ac93ba.

[17] M.A.A. Mahbub, A. Mulyadewi, C.G. Adios, A. Sumboja, Sustainable chicken manure-derived Carbon as a metalfree bifunctional electrocatalyst in zn-air battery, AIP Conf. Proc. 2652 (2022) 040011, https://doi.org/10.1063/5.0106289.

[18] B. He, Y. Deng, H. Wang, R. Wang, J. Jin, Y. Gong, L. Zhao, Metal organic framework derived perovskite/spinel heterojunction as efficient bifunctional oxygen electrocatalyst for rechargeable and flexible zn-air batteries, J. Colloid Interface Sci. 625 (2022) 502–511, https://doi.org/10.1016/j.jcis.2022.06.048.

[19] H. Lei, L. Ma, Q. Wan, Z. Huangfu, S. Tan, Z. Wang, W. Mai, Porous carbon nanofibers confined NiFe alloy nanoparticles as efficient bifunctional electrocatalysts for zn-air batteries, Nano Energy 104 (2022) 107941, https://doi.org/10.1016/j.nanoen.2022.107941.

[20] H. Li, S. Askari, J. Wang, N. Wolff, M. Behrens, L. Kienle, J. Benedikt, Nitrogen-doped NiCo2O4 nanowires on carbon paper as a self-supported air cathode for rechargeable zn-air batteries, Int. J. Hydrogen Energy 48 (2023) 26107–26118, https://doi.org/10.1016/j.ijhydene.2023.03.146.

[21] E.V. Rebrov, P.Z. Gao, Molecular catalysts for OER/ORR in Zn–Air batteries, Catalysts 13 (2023) 1289, https://doi.org/10.3390/catal13091289.

[22] R.S. Kumar, S. Prabhakaran, S. Ramakrishnan, S.C. Karthikeyan, A.R. Kim, D. H. Kim, D.J. Yoo, Developing outstanding bifunctional electrocatalysts for Rechargeable zn-air batteries using high-purity SpinelType $ZnCo_2Se_4$ Nanoparticles, Small 19 (2023) 2207096, https://doi.org/10.1002/smll.202207096.

[23] R.K. Mishra, K. Mohanty, A review of the next-generation biochar production from waste biomass for material applications, Sci. Total Environ. 904 (2023) 167171, https://doi.org/10.1016/j.scitotenv.2023.167171.

[24] C.D. Venkatachalam, S. Sekar, M. Sengottian, S.R. Ravichandran, P. Bhuvaneshwaran, A critical review of the production, activation, and morphological characteristic study on functionalized biochar, J. Storage Mater. 67 (2023) 107525, https://doi.org/10.1016/j.est.2023.107525.

[25] S. Rawat, C.T. Wang, C.H. Lay, S. Hotha, T. Bhaskar, Sustainable biochar for advanced electrochemical/energy storage applications, J. Storage Mater. 63 (2023) 107115, https://doi.org/10.1016/j.est.2023.107115.

[26] S. Han, S. Peng, Z. Gao, M. Sun, G. Cheng, H. Zhang, X. Su, M. Chen, L. Yu, Green bridge between waste and energy: conversion the rotten wood into cathode for functional zn-air battery, Electrochim. Acta 424 (2022) 140667, https://doi.org/10.1016/j.electacta.2022.140667.

[27] W. Miao, W. Liu, Y. Ding, R. Guo, J. Zhao, Y. Zhu, H. Yu, Y. Zhu, Cobalt (iron), nitrogen and carbon doped mushroom biochar for high-efficiency oxygen reduction in microbial fuel cell and zn-air battery, J. Environ. Chem. Eng. 10 (2022) 108474, https://doi.org/10.1016/j.jece.2022.108474.

[28] M. Tripath, J.N. Sahu, P. Ganesan, Effect of process parameters on production of biochar from biomass waste through pyrolysis: a review, Renew. Sustain. Energy Rev. 55 (2016) 467–481, https://doi.org/10.1016/j.rser.2015.10.122.

[29] Q. Zou, Corn-straw-converted activated carbons with tunable porosity and N/O functionalities as high-performance supercapacitors electrode at commercial-level mass loading, J. Storage Mater. 72 (2023) 108673, https://doi.org/10.1016/j.est.2023.108673.

[30] R. Mehdi, S.R. Naqvi, A.H. Khoja, R. Hussain, Biomass derived activated carbon by chemical surface modification as a source of clean energy for supercapacitor application, Fuel 348 (2023) 128529, https://doi.org/10.1016/j.fuel.2023.128529.

[31] D. Kalampaliki, G.D.T.M. Jayasingheb, E. Avramiotisa, I.D. Manariotis, D. Venieri, S.G. Poulopoulos, J. Szpunar, J. Vakros, D. Mantzavinos, Application of a KOH-activated biochar for the activation of persulfate and the degradation of sulfamethoxazole, Chem. Eng. Res. Des. 194 (2023) 306–317, https://doi.org/10.1016/j.cherd.2023.04.056.

[32] C.F. Xue, X.Q. Li, J.Q. Du, L.F. Wang, X.H. Li, W.J. Yan, X.G. Hao, Self-graphenized biochar with huge pore volume prepared from pre-boiled Ulva lactuca for electrochemical supercapacitor with high energy density, J. Storage Mater. 72 (2023) 108498, https://doi.org/10.1016/j.est.2023.108498.

[33] M. Guan, G. Wang, C. Yong, Y. Zhu, Y. Li, D. Zhu, Q. Jia, A novel composite hard carbon from waste Camellia oleifera shell modified by phenol-formaldehyde resin for supercapacitor electrode with high specific capacitance, Diam. Relat. Mater. 138 (2023) 110248, https://doi.org/10.1016/j.diamond.2023.110248.

[34] T.S. Andrade, J. Vakros, D. Mantzavinos, P. Lianos, Biochar obtained by carbonization of spent coffee grounds and its application in the construction of an energy storage device, Chemical Engineering Journal Advances 4 (2020) 100061, https://doi.org/10.1016/j.ceja.2020.100061.

[35] J. Vakros, I.D. Manariotis, V. Dracopoulos, D. Mantzavinos, P. Lianos, Biochar from spent malt rootlets and its application to an energy conversion and storage Device, Chemosensors 9 (2021) 57, https://doi.org/10.3390/chemosensors9030057.

[36] R. Dhawle, J. Vakros, V. Dracopoulos, I.D. Manariotis, D. Mantzavinos, P. Lianos, Enhancement of the photoelectrochemical production of hydrogen peroxide under intermittent light supply in the presence of an optimized biochar supercapacitor, Electrochim. Acta 427 (2022) 140846, https://doi.org/10.1016/j.electacta.2022.140846.

[37] S. Giannakopoulos, J. Vakros, V. Dracopoulos, I.D. Manarioti, D. Mantzavinos, P. Lianos, Enhancement of the photoelectrocatalytic degradation rate of a pollutant in the presence of a supercapacitor, J. Clean. Prod. 377 (2022) 134456, https://doi.org/10.1016/j.jclepro.2022.134456.

[38] S. Giannakopoulos, J. Vakros, I.D. Manarioti, D. Mantzavinos, P. Lianos, Study of the functionalities of a Biochar electrode combined with a photoelectrochemical cell, Materials 16 (2023) 43, https://doi.org/10.3390/ma16010043.

[39] Z. Wei, Y. Wei, Y. Liu, S. Niu, Y. Xu, J.H. Park, J.J. Wang, Biochar-based materials as remediation strategy in petroleum hydrocarbon-contaminated soil and water: performances, mechanisms, and environmental impact, J. Environ. Sci. 138 (2024) 350–372, https://doi.org/10.1016/j.jes.2023.04.008.

[40] K.H.H. Aziz, R. Kareem, Recent advances in water remediation from toxic heavy metals using biochar as a green and efficient adsorbent: a review, Case Studies in Chemical and Environmental Engineering 8 (2023) 100495, https://doi.org/10.1016/j.cscee.2023.100495.

[41] R. Suresh, L. Gnanasekaran, S. Rajendran, A.A. Jalil, M. Soto-Moscoso, K.S. Khoo, Z. Ma, H.S.H. Munawaroh, P.L. Show, Biomass waste as an alternative source of carbon and silicon-based absorbents for CO2 capturing application, Chemosphere 343 (2023) 140173, https://doi.org/10.1016/j.chemosphere.2023.140173.

[42] S. Giannakopoulos, Z. Frontistis, J. Vakros, S.G. Poulopoulos, I.D. Manariotis, D. Mantzavinos, Combined activation of persulfate by biochars and artificial light for the degradation of sulfamethoxazole in aqueous matrices, J. Taiwan Inst. Chem. Eng. 136 (2022) 104440, https://doi.org/10.1016/j.jtice.2022.104440.

[43] J. Vakros, Biochars and Their Use as Transesterification Catalysts for Biodiesel Production: A Short Review Catalysts 8 (2018) 562, https://doi.org/10.3390/catal8110562.
[44] K. Fedorov, M. Plata-Gryl, J.A. Khan, G., Boczkaj ultrasound-assisted heterogeneous activation of persulfate and peroxymonosulfate by asphaltenes for the degradation of BTEX in water, Journal of Hazardous Materials 397 (2020) 122804, https://doi.org/10.1016/j.jhazmat.2020.122804.
[45] A. Zanias, Z. Frontistis, J. Vakros, O. Arvaniti, R. Ribeiro, A. Silva, J. Faria, H. Gomes, D. Mantzavinos, Degradation of methylparaben by sonocatalysis using a Co–Fe magnetic carbon xerogel, Ultrason. Sonochem. 64 (2020) 105045, https://doi.org/10.1016/j.ultsonch.2020.105045.
[46] R. Darvishi, Ch. Soltani, M. Naderi, G. Boczkaj, S. Jorfi, A. Khataee, Hybrid metal and non-metal activation of oxone by magnetite nanostructures co-immobilized with nano-carbon black to degrade tetracycline, in: Fenton and Electrochemical Enhancement with Bio-Assay, Separation and Purification Technology, 2021, p. 119055, https://doi.org/10.1016/j.seppur.2021.119055.
[47] A. Alkhtib, M. Muna, E. Burton, J. Wamatu, M. Darag, E. Alkhaled, Z. Al-asa'ad, H. Almoufachi, R. Zaeowd, Effect of olive tree leaves and twigs on intake, digestibility, growth performance and blood variables of shami goats, Veterinary Medicine and Science 7 (2021) 908–914, https://doi.org/10.1002/vms3.419.
[48] P. Ntzoufra, J. Vakros, Z. Frontistis, S. Tsatsos, G. Kyriakou, S. Kennou, I. D. Manariotis, D. Mantzavinos, Effect of sodium persulfate treatment on the physicochemical properties and catalytic activity of biochar prepared from spent malt rootlets, J. Environ. Chem. Eng. 9 (2021) 105071, https://doi.org/10.1016/j.jece.2021.105071.
[49] M. Ntaflou, J. Vakros, Transesterification activity of modified biochars from spent malt rootlets using triacetin, J. Clean. Prod. 259 (2020) 120931, https://doi.org/10.1016/j.jclepro.2020.120931.
[50] L. Qian, F. Guo, X. Jia, Y. Zhan, H. Zhou, X. Jiang, C. Tao, Recent development in the synthesis of agricultural and forestry biomass–derived porous carbons for super– capacitor applications: a review, Ionics (kiel) 26 (2020) 3705–3723, https://doi.org/10.1007/s11581-020-03626-1.
[51] G. Gao, L.Z. Cheong, D. Wang, C. Shen, Pyrolytic carbon derived from spent coffee grounds as anode for sodium–ion batteries, Carbon Resour. Convers. 1 (2018) 104–108, https://doi.org/10.1016/j.crcon.2018.04.001.
[52] J. Kiefer, A. Stärk, A. Kiefer, H. Glade, Infrared spectroscopic analysis of the inorganic deposits from water in domestic and technical heat exchangers, Energies 11 (2018) 798, https://doi.org/10.3390/en11040798.
[53] E. Magioglou, Z. Frontistis, J. Vakros, I.D. Manariotis, D. Mantzavinos, Activation of persulfate by Biochars from valorized olive stones for the degradation of sulfamethoxazole, Catalysts 9 (2019) 419, https://doi.org/10.3390/catal9050419.
[54] E. Grilla, J. Vakros, I. Konstantinou, I.D. Manariotis, D. Mantzavinos, Activation of persulfate by biochar from spent malt rootlets for the degradation of trimethoprim in the presence of inorganic ions, J. Chem. Technol. Biotechnol. 95 (2020) 2348–2358, https://doi.org/10.1002/jctb.6513.
[55] J. Wang, S. Kaskel, KOH activation of carbon-based materials for energy storage, J. Mater. Chem. 22 (2012) 23710–23725, https://doi.org/10.1039/C2JM34066F.
[56] W.J. Liu, H. Jiang, H.Q. Yu, Emerging applications of biochar-based materials for energy storage and conversion, Energ. Environ. Sci. 12 (2019) 1751–1779, https://doi.org/10.1039/C9EE00206E.
[57] S. Yadav, A. Ahmad, M. Priyadarshini, B.K. Dubey, M.M. Ghangrekar, Transition towards Renewable Nano-Carbon-Based Electrocatalysts in Electrochemical and Bio-Electrochemical Technologies FlatChem 44 (2024) 100623, https://doi.org/10.1016/j.flatc.2024.100623.
[58] J. Yang, S. Tang, W. Mei, Y. Chen, W. Yi, P. Lv, G. Yang, Valorising lignocellulosic biomass to high-performance electrocatalysts via anaerobic digestion pretreatment, Biochar 6 (2024) 23, https://doi.org/10.1007/s42773-024-00311-8.
[59] S. Pérez-Rodríguez, O. Pinto, M.T. Izquierdo, C. Segura, P.S. Poon, A. Celzard, J. Matos, V. Fierro, Upgrading of pine tannin biochars as electrochemical capacitor electrodes, J. Colloid Interface Sci. 601 (2021) 863–876, https://doi.org/10.1016/j.jcis.2021.05.162.
[60] C. Li, K. Cao, Y. Fan, Q. Li, Y. Zhang, Z. Guo, Kinetically well-matched porous framework dual carbon electrodes for high-performance sodium-ion hybrid capacitors, J. Colloid Interface Sci. 652 (2023) 1356–1366, https://doi.org/10.1016/j.jcis.2023.08.162.
[61] A.P. Khedulkar, V.D. Dang, B. Pandit, T.A.N. Bui, H.L. Tran, R. Doong, Flower-like nickel hydroxide@tea leaf-derived biochar composite for high-performance supercapacitor application, J. Colloid Interface Sci. 623 (2022) 845–855, https://doi.org/10.1016/j.jcis.2022.04.178.
[62] X. Lin, L. Xue, B. Liu, X. Qiu, J. Liu, X. Wang, Y. Qi, Y. Qin, Lignosulfonate-assisted in situ synthesis of Co9S8–Ni3S2 heterojunctions encapsulated by S/N co-doped biochar for efficient water oxidation, J. Colloid Interface Sci. 644 (2023) 295–303, https://doi.org/10.1016/j.jcis.2023.04.070.
[63] J. Wang, L. Wu, L. Shen, Q. Zhou, Y. Chen, J. Wu, Y. Wen, J. Zheng, CoO embedded porous biomass-derived carbon as dual-functional host material for lithium-sulfur batteries, J. Colloid Interface Sci. 640 (2023) 415–422, https://doi.org/10.1016/j.jcis.2023.02.123.
[64] S. Han, Y. Wu, S. Peng, Y. Xu, M. Sun, X. Su, Y. Zhong, H. Wen, J. He, L. Yu, Boosting the electrochemical performance of zn-air battery with N/O codoped biochar catalyst via a simple physical strategy of forced convection intensity, Chem. Eng. Sci. 272 (2023) 118615, https://doi.org/10.1016/j.ces.2023.118615.